

Skyrmionic Transport and First Order Phase Transitions in Twisted Bilayer Graphene Quantum Hall Ferromagnet

Vineet Pandey,[†] Prasenjit Ghosh,[†] Riju Pal,[‡] Sourav Paul,[†] Abhijith M B,[†] Kenji Watanabe,[¶] Takashi Taniguchi,[§] Atindra Nath Pal,[‡] and Vidya Kochat^{*,†}

[†]*Materials Science Centre, Indian Institute of Technology, Kharagpur, West Bengal - 721302, India*

[‡]*S. N. Bose National Centre for Basic Sciences, Kolkata, West Bengal -700106, India*

[¶]*Research Center for Electronic and Optical Materials, National Institute for Materials Science, 1-1 Namiki, Tsukuba 305-0044, Japan*

[§]*Research Center for Materials Nanoarchitectonics, National Institute for Materials Science, 1-1 Namiki, Tsukuba 305-0044, Japan*

E-mail: vidya@matssc.iitkgp.ac.in

Abstract

Large-angle twisted bilayer graphene (TBLG) realizes a multicomponent quantum Hall (QH) platform of spin, valley and layer pseudospins with strong Coulomb interaction-driven symmetry broken phases. Here, we investigate the low energy Landau-level spectrum of layer-decoupled TBLG and identify skyrmion-textured charged excitations and a field-induced insulating transition to an intervalley coherent state at zero-filling factor. Symmetric potential difference perpendicular to TBLG demonstrated layer coherent population of ground states with uniform energy barriers, while the charge imbalance in the layers at finite displacement

field led to multidomain nucleation and a pronounced hysteresis in the exchange-dominated transport regime suggesting first order phase transitions between different QH ferromagnetic ground states.

Keywords: twisted bilayer graphene, broken symmetry states, Quantum Hall Ferromagnetism, skyrmions.

Multicomponent Quantum Hall (QH) physics arises from various degeneracies underlying the Hamiltonian of the material system resulting in additional pseudospin/isospin degrees of freedom such as the electron spin, valley index in multi-valley materials, the sub-band and layer index in 2D electron gas systems (2DEGS) with multiple quantum well structures or 2D bilayers.¹⁻⁴ The spatial ordering of pseudospin/isospin degrees of freedom led to a new class of condensed matter systems termed as QH Ferromagnets.⁵ In modulation-doped semiconductor heterostructures and double quantum wells, as the interlayer separation (d) approaches the magnetic length (l_B), interlayer Coulomb coupling stabilizes excitonic, interlayer-coherent order and results in anomalous transport.⁶⁻¹⁰ The strong Coulomb interaction in the lower LLs results in a large exchange energy favouring parallel spins, which dominates the Zeeman energy term and leads to energetically favourable skyrmion excitations observed in various 2DEGS and 2D bilayers.¹¹⁻¹³ Similar QH ferromagnetic phases characterized by interaction-induced gaps and broken symmetries at integer filling factors have been observed in various graphene systems such as single/bi/tri/rhombohedral stacked multilayer graphene attributed to the spin-valley degeneracy in graphene.¹⁴⁻²⁴

The low energy band structure of monolayer graphene is described by two flavours of massless Dirac fermions at the inequivalent K and K' valleys of the hexagonal Brillouin zone giving rise to the anomalous QH sequence of $\sigma_{xy} = \pm \frac{4e^2}{h} \left(N + \frac{1}{2} \right)$ due to four-fold spin-valley degeneracy.^{25,26} Thus the graphene LL is described by a single $SU(4)$ pseudospin and gives rise to ferromagnetic instabilities driven by exchange interactions, with order parameter corresponding to a finite polarization in spin and/or valley space. This results in finite charge excitation gaps at integer filling factors within the quartet LL manifested as QH pseudospin ferromagnetic states.^{14,27,28} TBLG can be considered as a unique bilayer 2DEG with two mutually rotated single layers with interlayer Coulomb interactions and tunnelling in the extremity of a sub-nm tunnel barrier of 0.4 nm. At twist angles of 1.05° , called the magic angles, interlayer hybridization of Dirac cones produces flat bands, thereby leading to strong coupling of the layers.²⁹⁻³¹ At larger twist angles, the Dirac cones of each layer are significantly displaced in the momentum space and this resultant momentum mismatch strongly suppresses interlayer tunnelling. In the large-angle

limit, the layer quantum number is approximately conserved, so each Landau level becomes an eight-fold manifold (spin \times valley \times layer) that widens the set of competing pseudospin orders to include layer-polarized ferromagnets, interlayer-coherent excitonic condensates, valley-ordered textures, and mixed spin-valley states.^{18,32–34} Experimentally, large-angle devices show stable odd-integer interlayer-coherent states, a hierarchy of integer and fractional incompressible phases that respond to layer imbalance, and notably large gaps for interlayer-correlated phases.^{33,35–41} Here we present a systematic study of tilted-field and displacement-resolved QH transport in high-mobility single- and dual-gated large-angle TBLG focused on the interaction-driven symmetry breaking in the eightfold degenerate LLs of TBLG. Asymmetric screening produces uneven layer filling and multi-domain network of QH ferromagnetic ground states. Tilted field activation gap studies reveal the presence of charged spin/valley skyrmions in the low energy LL spectrum which transition from smooth skyrmion textures to metastable domain walls through first order phase transitions at finite displacement fields.

The large-angle TBLG devices in h-BN encapsulated Hall bar geometry were fabricated using the van der Waals pick-up and stack, followed by edge contact technique.⁴² Randomly stacked TBLG heterostructures were characterized using Raman spectroscopy and the twist angles were estimated to be $\sim 5^\circ$ and 8° for devices D1 and D2 respectively.^{43,44} Fig. 1(a) depicts the measurement configuration for bottom-gated h-BN/TBLG/h-BN device D1, while device D2 was fabricated as a dual-gated structure. Both the devices had mobilities of $\sim 2,00,000$ cm²/Vs and displayed well-resolved QH plateaus at magnetic fields as low as 1 T. The Landau fan diagram showing the evolution of R_{xx} minima in magnetic field (B) along with back gate modulation of Fermi level, E_F is shown in Fig. 1(b) for D1. The integer QHE is observed with R_{xx} minima at LL filling factors given by $\nu_{\text{tot}} = \pm 4, \pm 8, \pm 12, \pm 16, \dots$ indicating the presence of an eight-fold degenerate zero Landau level, with additional minima in the $N = 0, 1$ LLs arising from broken symmetry states. The low density of states in graphene leads to incomplete screening of the gate field by the bottom graphene layer, resulting in different charge carrier densities in the upper and lower graphene layers of D1. This results in a beating pattern in the Shubnikov-de Haas (SdH) os-

cillations measured in the R_{xx} of D1 as illustrated in Fig. 1(c). The Fast Fourier Transform (FFT) of ΔR_{xx} (R_{xx} oscillations centered around zero) vs. $1/B$ performed for different total carrier densities, n_{tot} yields two prominent peaks corresponding to the two frequencies ($f_{U,L}$ for upper and lower layers) involved in the SdH oscillations as shown in Fig. 1(c). This translates to the carrier densities of upper and lower layers defined as n_U and n_L through the relation $n_{U,L} = g e f_{U,L} / h$, where g is the degeneracy factor of 4 arising from four-fold spin-valley degeneracy in each graphene layer, which is plotted in Fig. 1(d) along with n_{tot} , where $n_{tot} = n_U + n_L$. These carrier density values can be fitted using a model of independently contacted graphene double layers separated by a thin dielectric.^{32,45,46}

$$E_F(n_L) = \frac{e^2 n_U}{C_{int}} + E_F(n_U) \quad (1)$$

where C_{int} is the interlayer capacitance of TBLG, whose value can be estimated from the fit to be $5.7 \pm 1 \mu\text{F cm}^{-2}$.⁴⁷

In large-angle TBLG, the interlayer Coulomb interactions modulated by the carrier density in individual layers can compete with the magnetic field-tuned intralayer Coulomb interactions. This competition can result in new ground states and phase transitions in the QH ferromagnetic regime of TBLG. Fig. 2(a) shows the magnetic field evolution of the integer QH states as the Fermi level is tuned from electron to hole filling for D1 at 1.6 K. A magnetic field-induced QH insulator phase was observed at $\nu_{tot} = 0$ along with additional R_{xx} minima within the eight-fold degenerate $N = 0$ LL and at integer fillings in the higher LLs, signifying emergence of broken symmetry QH phases at high magnetic fields.⁴⁸ The QH insulator gap at $\nu_{tot} = 0$, Δ^0 increases linearly with magnetic field B as shown in Fig. 2(b) inset, analogous to SLG.⁴⁹ In device D1 illustrated in Fig. 2(b), $R_0 \sim \xi(h^2)$, with R_0 being the R_{xx} at $\nu_{tot} = 0$ and ξ the correlation length which has Kosterlitz-Thouless (KT) dependence given by^{50,51}

$$\xi_{KT} \sim \exp(b/\sqrt{1-h}) \quad (2)$$

where $h = B/B_C$ with $B_C \sim 12 \text{ T}$.⁴⁷ In Fig. 2(b), the high- B region is linear with slope, $b \sim 0.79$,

which agrees well with standard KT theory.⁵¹ This also concurs with the recent scanning tunneling spectroscopic (STS) studies indicating magnetic field-tuned transition to an intervalley coherent state (IVC) with a Kekulé reconstruction, in which the LL associated with the K and K' valleys localize on B and A sublattices respectively.^{48,52–55} In the high B limit, the ground state is an XY ordered phase formed from charge-neutral bound vortex-antivortex (V-AV) pairs, in which the Coulomb exchange favours fully valley-polarized state. Unbinding of V-AV pairs triggers KT transition to a disordered phase at low B .⁵⁰ Our experiment demonstrates that even in the limit of sub-nm interlayer spacing, each graphene layer in the TBLG preserves their individual pseudospin magnetic ground states at $\nu_{\text{tot}} = 0$.

The tilted field studies of activation gaps at integer filling factors, Δ^{ν} , as shown in Fig. 2(c) and Fig. 2(d) helped to identify the signatures of spin textures of the ground states of the broken symmetry states in the $N = 0$ LL. The spin responds to the total magnetic field, B , independent of the direction, unlike the orbital effects that depend only on the out-of-plane component, $B_p = B \cos \theta$.^{14,16,17,56,57} At a fixed B , increasing the tilt angle θ of the sample reduces the B_p and weakens the gaps, which is shown in Fig. 2(c) for $B = 11$ T. The R_0 plotted as a function of B_p estimated from a range of B and θ values is shown in the inset of Fig. 2(c). From these traces we observe that R_0 decreases as the in-plane field grows (higher θ) even though B increases, indicating a spin-unpolarized insulating phase which is a further confirmation of the formation of IVC state at high B .¹⁴ The calculated activation gaps extracted from the Arrhenius fit of ρ_{xx} , Δ^{ν} , for the broken symmetry states at $\nu_{\text{tot}} = 1, 2, 3$ as a function of B is plotted in Fig. 2(d) for a fixed B_p of 6 T, by varying θ . Δ^1 and Δ^2 exhibit a linear dependence on B , suggesting a spin-polarized ground state. Whereas, the negligible dependence of Δ^3 on B suggests spin-unpolarized, valley textured excitations. The Δ for $\nu_{\text{tot}} = 1, 2$ can be fitted with the gap equation^{11,14,58–60}

$$\Delta = \Delta_X(B_p, K) + (2K + 1) g_0 \mu_B B - \Gamma \quad (3)$$

where $\Delta_X(B_p, K)$ is the exchange energy and typically scales with the Coulomb energy $E_C \sim$

$\frac{e^2}{4\pi\epsilon\ell_B}$, $l_B \propto 1/\sqrt{B_p}$, g_0 is the bare Landé g -factor (≈ 2 in graphene), μ_B is the Bohr magneton and Γ is the disorder broadening of the Landau levels. The second term is the Zeeman energy gap modified by the parameter K , where $K \geq 0$ represents the number of extra spins flipped in a skyrmion texture beyond the single spin flip of a conventional particle-hole excitation. For $K = 0$, the excitation is a single spin flip and the slope gives $g_{\parallel} \approx g_0$, where g_{\parallel} is defined as $g_{\parallel} \equiv \frac{1}{\mu_B} \partial_B \Delta$, whereas for $K > 0$, multiple flipped spins lead to $g_{\parallel} > g_0$, a hallmark of exchange-dominated skyrmionic transport.^{14,59} The fit to the measured values of $\Delta^{1,2}$ yielded g_{\parallel} values of 7.92 and 5.96 for $\nu_{\text{tot}} = 1$ and 2 respectively, indicating that the lowest-energy excitations involve spin skyrmion textures. Our findings indicate that the low energy excitations in decoupled TBLG are of similar nature as observed in SLG, where the lowest energy excitations are skyrmions in spin-valley space for $N \leq 3$ where exchange energy dominates Zeeman anisotropy.^{28,61}

The evolution of integer QH states and the appearance of broken symmetry states was observed to depend remarkably on the direction of the gate voltage sweep direction as shown in Fig. 3(a) and Fig. 3(b). The notable features here are the asymmetry in the emergence of broken symmetry states on the electron and hole sides as well as a considerable hysteresis which is developed in the lower LL regime where $-8 \leq \nu_{\text{tot}} \leq 8$. We also note that the hysteresis develops only at low temperatures and high B , signified by the absence of hysteresis at low field of 3 T and at temperatures greater than 15 K as can be seen from the plots of R_{xx} and hall conductance, σ_{xy} as a function of total filling factor, ν_{tot} in Fig. 3(c) and Fig. 3(d). The temperature scale where the hysteresis vanishes corresponds to the energy scale for pseudospin-pseudospin interaction energy which is of the order ~ 1.5 meV calculated from the hysteresis range. This strongly suggests that the hysteresis is a consequence of the QH ferromagnetism developed in TBLG and is present in the QH regime of broken symmetry states where the transport is dominated by spin/valley skyrmion excitations. STS studies have shown direct observation of topological excitations of the IVC phase at $\nu_{\text{tot}} = 0$ by visualizing valley skyrmions near charged defects, whose valley texture resembles canted antiferromagnetic skyrmion excitation of the Kekulé order.^{52,53,62} In graphene LL at $\nu = \pm 1$, corresponding to quarter filling, where Zeeman anisotropy is not dominant, all the electrons

(or holes) spontaneously align their spin to reduce the Coulomb interaction. Instead of spin-flip transitions, this spin-polarization happens through formation of skyrmions carrying a charge of $\pm e$ due to their lower energy.^{14,28} In contrast, for $N \neq 0$ with dominant Zeeman anisotropy, spin polarized ground states occur at half-filling and charged excitations with valley flip textures at quarter filling.¹⁴ The role of charge imbalance between the graphene layers and the skyrmion evolution as possible origins of QH hysteresis was further comprehensively explored in dual-gated structures.

In dual-gated TBLG device, D2, the total charge carrier density and displacement field perpendicular to the layers can be independently controlled. Here the opposite gate sweep directions at 0 T showed no visible hysteresis at any D .⁴⁷ At high values of B , QH ferromagnetic states were observed with marked differences between $D/\epsilon_0 = 0$ and $|D/\epsilon_0| \neq 0$ as shown in Fig. 4(a), with R_{xx} minima at $|v_{\text{tot}}| = 1, 3$ absent when $D/\epsilon_0 = 0$, but emerges at finite D . At $D/\epsilon_0 = 0$, when both the graphene layers are charge neutral ($v_{\text{tot}} = 0$), we observe an insulating state that can be attributed to the IVC states in the individual graphene layers. Increasing the v_{tot} at $D/\epsilon_0 = 0$ results in filling of the LLs in the upper and lower graphene layers in a coherent manner, resulting in R_{xx} minima at $v_{\text{tot}} = 2, 4$ corresponding to quarter-filled and fully-filled LLs respectively of individual layers. Applying a perpendicular D explicitly breaks layer degeneracy and produces an easy-axis anisotropy that energetically favors one layer, where the intra-layer exchange readily polarizes the spin-valley flavours in the favoured layer and odd fillings at $v_{\text{tot}} = 1, 3$ appear.^{33,35,38} The full spectrum of broken symmetry states observed in the filling of lowest LL in TBLG system is shown in Fig. 4(b). Another interesting observation here is that the hysteresis is completely absent when $D/\epsilon_0 = 0$, but increases with D and can be observed till $v_{\text{tot}} = 12$ at the highest accessible D in D2 device. The pseudospin polarization in the spin-valley space of the graphene layers leads to Ising ferromagnetism, with inevitable nucleation of multiple domains in the presence of disorder or at finite temperature.^{63,64} When both layers are filled coherently as for the case of $D/\epsilon_0 = 0$, the ferromagnetic ground states as well as the lowest energy excitations in both layers are analogous forming a uniform potential landscape. This favours continuous rotation of the pseudospin polar-

ization without creating sharp domain boundaries and with reversible reconfiguration with opposite gate sweep directions. A finite displacement field results in charge imbalance between the layers that alters the energy landscape in the layers differently through screening of the residual disorder in individual layers. This results in the formation of pseudospin ordered domains and disorder nucleated domains of low energy excitations of skyrmions, separated by domain walls, where the pseudospin index (spin, valley) is different in the sublayers.⁶⁵ The hysteresis observed at finite D indicates first-order phase transitions between the various magnetic ground states as a particular broken symmetry state is approached.^{5,10,63,66,67} It specifically depends on the initial pseudospin index configuration of the sublayers which have energetically different anisotropy barriers during opposite gate sweep directions, analogous to a memory effect based on the history of gate sweep direction. The hysteretic behaviour is observed only in exchange-dominated transport regime with skyrmionic low energy excitations whose size scales down with increasing disorder that weakens long-range spin/pseudospin interactions. Further evidence is provided by the absence of hysteresis in a device, D3 with relatively larger disorder, at field of 9 T and 1.6 K.⁴⁷ Here the QH ferromagnetic states were not visible due to larger disorder strength which rapidly shrinks the domain sizes under similar experimental conditions.

In conclusion, we observe the interplay of charge screening effects, broken symmetry states and multidomain physics in the QH ferromagnetic regime of decoupled TBLG. The exchange interaction energy scale dominates the low energy transport, resulting in ferromagnetic QH ground states with lowest energy excitations of skyrmion texture in spin-valley pseudospin space as inferred from tilted field activation gaps. Investigation of dual-gated TBLG devices demonstrated layer coherent population of ground states with uniform energy barriers at zero displacement fields, while the charge imbalance in the layers at finite displacement field led to multidomain nucleation and hysteresis between different QH ferromagnetic ground states driven by first order phase transitions. Our work paves way for understanding symmetry breaking phases in distinctly stacked multilayer graphene and Moiré systems.

Acknowledgement

V.P., P.G., S.P., A.M.B and V.K. acknowledge funding support from the DST-Nanomission programme of the Department of Science and Technology, Government of India (DST/NM/TUE/QM-1/2019) and the STEP facility, IIT Kharagpur. R.P. and A.N.P. acknowledge the Thematic Unit of Excellence on Nanodevice Technology (grant no. SR/NM/NS-09/2011) and the Technical Research Centre (TRC) Instrument facilities of S. N. Bose National Centre for Basic Sciences, established under the TRC project of Department of Science and Technology (DST), Govt. of India. A.N.P. acknowledges DST Nano Mission: DST/NM/TUE/QM-10/2019. K.W. and T.T. acknowledge support from the JSPS KAKENHI (Grant Numbers 21H05233 and 23H02052), the CREST (JPMJCR24A5), JST and World Premier International Research Center Initiative (WPI), MEXT, Japan.

References

- (1) Girvin, S. M. Spin and Isospin: Exotic Order in Quantum Hall Ferromagnets. *Physics Today* **2000**, *53*, 39–45.
- (2) Jungwirth, T.; Shukla, S. P.; Smrčka, L.; Shayegan, M.; MacDonald, A. H. Magnetic Anisotropy in Quantum Hall Ferromagnets. *Physical Review Letters* **1998**, *81*, 2328–2331.
- (3) Daneshvar, A. J.; Ford, C. J. B.; Simmons, M. Y.; Khaetskii, A. V.; Hamilton, A. R.; Pepper, M.; Ritchie, D. A. Magnetization Instability in a Two-Dimensional System. *Physical Review Letters* **1997**, *79*, 4449–4452.
- (4) Pellegrini, V.; Pinczuk, A.; Dennis, B. S.; Plaut, A. S.; Pfeiffer, L. N.; West, K. W. Evidence of Soft-Mode Quantum Phase Transitions in Electron Double Layers. *Science* **1998**, *281*, 799–802.
- (5) Eom, J.; Cho, H.; Kang, W.; Campman, K. L.; Gossard, A. C.; Bichler, M.; Wegscheider, W.

- Quantum Hall Ferromagnetism in a Two-Dimensional Electron System. *Science* **2000**, 289, 2320–2323.
- (6) Spielman, I. B.; Eisenstein, J. P.; Pfeiffer, L. N.; West, K. W. Resonantly Enhanced Tunneling in a Double Layer Quantum Hall Ferromagnet. *Physical Review Letters* **2000**, 84, 5808–5811.
- (7) Murphy, S. Q.; Eisenstein, J. P.; Boebinger, G. S.; Pfeiffer, L. N.; West, K. W. Many-body integer quantum Hall effect: Evidence for new phase transitions. *Physical Review Letters* **1994**, 72, 728–731.
- (8) Eisenstein, J. P.; MacDonald, A. H. Bose–Einstein condensation of excitons in bilayer electron systems. *Nature* **2004**, 432, 691–694.
- (9) Wiersma, R. D.; Lok, J. G. S.; Kraus, S.; Dietsche, W.; von Klitzing, K.; Schuh, D.; Bichler, M.; Tranitz, H.-P.; Wegscheider, W. Activated Transport in the Separate Layers that Form the $\nu_T = 1$ Exciton Condensate. *Physical Review Letters* **2004**, 93, 266805.
- (10) Poortere, E. P. D.; Tutuc, E.; Papadakis, S. J.; Shayegan, M. Resistance Spikes at Transitions Between Quantum Hall Ferromagnets. *Science* **2000**, 290, 1546–1549.
- (11) Sondhi, S. L.; Karlhede, A.; Kivelson, S. A.; Rezayi, E. H. Skyrmions and the crossover from the integer to fractional quantum Hall effect at small Zeeman energies. *Physical Review B* **1993**, 47, 16419–16426.
- (12) Tycko, R.; Barrett, S. E.; Dabbagh, G.; Pfeiffer, L. N.; West, K. W. Electronic States in Gallium Arsenide Quantum Wells Probed by Optically Pumped NMR. *Science* **1995**, 268, 1460–1463.
- (13) Sarma, S. D.; Pinczuk, A. Perspectives in Quantum Hall Effects: Novel Quantum Liquids in Low-Dimensional Semiconductor Structures. 1997.
- (14) Young, A. F.; Dean, C. R.; Wang, L.; Ren, H.; Cadden-Zimansky, P.; Watanabe, K.;

- Taniguchi, T.; Hone, J.; Shepard, K. L.; Kim, P. Spin and valley quantum Hall ferromagnetism in graphene. *Nature Physics* **2012**, *8*, 550–556.
- (15) Zhao, Y.; Cadden-Zimansky, P.; Jiang, Z.; Kim, P. Symmetry Breaking in the Zero-Energy Landau Level in Bilayer Graphene. *Physical Review Letters* **2010**, *104*, 066801.
- (16) Jiang, Z.; Zhang, Y.; Stormer, H. L.; Kim, P. Quantum Hall States near the Charge-Neutral Dirac Point in Graphene. *Physical Review Letters* **2007**, *99*, 106802.
- (17) Zhang, Y.; Jiang, Z.; Small, J. P.; Purewal, M. S.; Tan, Y.-W.; Fazlollahi, M.; Chudow, J. D.; Jaszczak, J. A.; Stormer, H. L.; Kim, P. Landau-Level Splitting in Graphene in High Magnetic Fields. *Physical Review Letters* **2006**, *96*, 136806.
- (18) Weitz, R. T.; Allen, M. T.; Feldman, B. E.; Martin, J.; Yacoby, A. Broken-Symmetry States in Doubly Gated Suspended Bilayer Graphene. *Science* **2010**, *330*, 812–816.
- (19) Feldman, B. E.; Martin, J.; Yacoby, A. Broken-symmetry states and divergent resistance in suspended bilayer graphene. *Nature Physics* **2009**, *5*, 889–893.
- (20) Datta, B.; Dey, S.; Samanta, A.; Agarwal, H.; Borah, A.; Watanabe, K.; Taniguchi, T.; Sensarma, R.; Deshmukh, M. M. Strong electronic interaction and multiple quantum Hall ferromagnetic phases in trilayer graphene. *Nature Communications* **2017**, *8*, 14518.
- (21) Lee, Y.; Velasco, J.; Tran, D.; Zhang, F.; Bao, W.; Jing, L.; Myhro, K.; Smirnov, D.; Lau, C. N. Broken Symmetry Quantum Hall States in Dual-Gated ABA Trilayer Graphene. *Nano Letters* **2013**, *13*, 1627–1631.
- (22) Liu, K.; Zheng, J.; Sha, Y.; Lyu, B.; Li, F.; Park, Y.; Ren, Y.; Watanabe, K.; Taniguchi, T.; Jia, J.; Luo, W.; Shi, Z.; Jung, J.; Chen, G. Spontaneous broken-symmetry insulator and metals in tetralayer rhombohedral graphene. *Nature Nanotechnology* **2024**, *19*, 188–195.
- (23) Han, T.; Lu, Z.; Scuri, G.; Sung, J.; Wang, J.; Han, T.; Watanabe, K.; Taniguchi, T.;

- Park, H.; Ju, L. Correlated insulator and Chern insulators in pentalayer rhombohedral-stacked graphene. *Nature Nanotechnology* **2024**, *19*, 181–187.
- (24) Lee, K.; Fallahazad, B.; Xue, J.; Dillen, D. C.; Kim, K.; Taniguchi, T.; Watanabe, K.; Tutuc, E. Chemical potential and quantum Hall ferromagnetism in bilayer graphene. *Science* **2014**, *345*, 58–61.
- (25) Novoselov, K. S.; Geim, A. K.; Morozov, S. V.; Jiang, D.; Katsnelson, M. I.; Grigorieva, I. V.; Dubonos, S. V.; Firsov, A. A. Two-dimensional gas of massless Dirac fermions in graphene. *Nature* **2005**, *438*, 197–200.
- (26) Zhang, Y.; Tan, Y.-W.; Stormer, H. L.; Kim, P. Experimental observation of the quantum Hall effect and Berry's phase in graphene. *Nature* **2005**, *438*, 201–204.
- (27) Nomura, K.; MacDonald, A. H. Quantum Hall Ferromagnetism in Graphene. *Physical Review Letters* **2006**, *96*, 256602.
- (28) Yang, K.; Sarma, S. D.; MacDonald, A. H. Collective modes and skyrmion excitations in graphene $SU(4)$ quantum Hall ferromagnets. *Physical Review B* **2006**, *74*, 075423.
- (29) Cao, Y.; Fatemi, V.; Fang, S.; Watanabe, K.; Taniguchi, T.; Kaxiras, E.; Jarillo-Herrero, P. Unconventional superconductivity in magic-angle graphene superlattices. *Nature* **2018**, *556*, 43–50.
- (30) Cao, Y.; Fatemi, V.; Demir, A.; Fang, S.; Tomarken, S. L.; Luo, J. Y.; Sanchez-Yamagishi, J. D.; Watanabe, K.; Taniguchi, T.; Kaxiras, E.; Ashoori, R. C.; Jarillo-Herrero, P. Correlated insulator behaviour at half-filling in magic-angle graphene superlattices. *Nature* **2018**, *556*, 80–84.
- (31) Bistritzer, R.; MacDonald, A. H. Moiré bands in twisted double-layer graphene. *Proceedings of the National Academy of Sciences* **2011**, *108*, 12233–12237.

- (32) Sanchez-Yamagishi, J. D.; Taychatanapat, T.; Watanabe, K.; Taniguchi, T.; Yacoby, A.; Jarillo-Herrero, P. Quantum Hall Effect, Screening, and Layer-Polarized Insulating States in Twisted Bilayer Graphene. *Physical Review Letters* **2012**, *108*, 076601.
- (33) Kim, D.; Kang, B.; Choi, Y.-B.; Watanabe, K.; Taniguchi, T.; Lee, G.-H.; Cho, G. Y.; Kim, Y. Robust Interlayer-Coherent Quantum Hall States in Twisted Bilayer Graphene. *Nano Letters* **2023**, *23*, 163–169.
- (34) Pezzini, S.; Mišeikis, V.; Piccinini, G.; Forti, S.; Pace, S.; Engelke, R.; Rossella, F.; Watanabe, K.; Taniguchi, T.; Kim, P.; Coletti, C. 30°-Twisted Bilayer Graphene Quasicrystals from Chemical Vapor Deposition. *Nano Letters* **2020**, *20*, 3313–3319.
- (35) Kim, Y.; Moon, P.; Watanabe, K.; Taniguchi, T.; Smet, J. H. Odd Integer Quantum Hall States with Interlayer Coherence in Twisted Bilayer Graphene. *Nano Letters* **2021**, *21*, 4249–4254.
- (36) Li, Q. et al. Strongly coupled magneto-exciton condensates in large-angle twisted double bilayer graphene. *Nature Communications* **2024**, *15*, 5065.
- (37) Yuan, Y.; Liu, L.; Zhu, J.; Dong, J.; Chu, Y.; Wu, F.; Du, L.; Watanabe, K.; Taniguchi, T.; Shi, D.; Zhang, G.; Yang, W. Interplay of Landau Quantization and Interminivalley Scatterings in a Weakly Coupled Moiré Superlattice. *Nano Letters* **2024**, *24*, 6722–6729.
- (38) Sanchez-Yamagishi, J. D.; Luo, J. Y.; Young, A. F.; Hunt, B. M.; Watanabe, K.; Taniguchi, T.; Ashoori, R. C.; Jarillo-Herrero, P. Helical edge states and fractional quantum Hall effect in a graphene electron–hole bilayer. *Nature Nanotechnology* **2017**, *12*, 118–122.
- (39) Kim, J. H.; Kang, S.-H.; Yoon, D.; Kim, H.; Kim, J.-S.; Haidari, M. M.; Jang, D. J.; Ko, J.-Y.; Son, Y.-W.; Park, B. H.; Choi, J. S. Twist angle-dependent transport properties of twisted bilayer graphene. *NPG Asia Materials* **2024**, *16*, 36.
- (40) Babich, I. et al. Milli-Tesla quantization enabled by tuneable Coulomb screening in large-angle twisted graphene. *Nature Communications* **2025**, *16*, 7389.

- (41) Kim, Y.; Park, J.; Song, I.; Ok, J. M.; Jo, Y.; Watanabe, K.; Taniguchi, T.; Choi, H. C.; Lee, D. S.; Jung, S.; Kim, J. S. Broken-Symmetry Quantum Hall States in Twisted Bilayer Graphene. *Scientific Reports* **2016**, *6*, 38068.
- (42) Wang, L.; Meric, I.; Huang, P. Y.; Gao, Q.; Gao, Y.; Tran, H.; Taniguchi, T.; Watanabe, K.; Campos, L. M.; Muller, D. A.; Guo, J.; Kim, P.; Hone, J.; Shepard, K. L.; Dean, C. R. One-Dimensional Electrical Contact to a Two-Dimensional Material. *Science* **2013**, *342*, 614–617.
- (43) Pandey, V.; Mishra, S.; Maity, N.; Paul, S.; B, A. M.; Roy, A. K.; Glavin, N. R.; Watanabe, K.; Taniguchi, T.; Singh, A. K.; Kochat, V. Probing Interlayer Interactions and Commensurate–Incommensurate Transition in Twisted Bilayer Graphene through Raman Spectroscopy. *ACS Nano* **2024**, *18*, 4756–4764.
- (44) Carozo, V.; Almeida, C. M.; Ferreira, E. H. M.; Cançado, L. G.; Achete, C. A.; Jorio, A. Raman Signature of Graphene Superlattices. *Nano Letters* **2011**, *11*, 4527–4534.
- (45) Fallahazad, B.; Hao, Y.; Lee, K.; Kim, S.; Ruoff, R. S.; Tutuc, E. Quantum Hall effect in Bernal stacked and twisted bilayer graphene grown on Cu by chemical vapor deposition. *Physical Review B* **2012**, *85*, 201408.
- (46) Schmidt, H.; Lüdtke, T.; Barthold, P.; McCann, E.; Fal’ko, V. I.; Haug, R. J. Tunable graphene system with two decoupled monolayers. *Applied Physics Letters* **2008**, *93*.
- (47) See Supplemental Material at [URL will be inserted by publisher] for additional experimental data like Experimental methods, two layer model of TBLG and D-dependent measurements at B=0T etc.
- (48) Kharitonov, M. Phase diagram for the $\nu = 0$ quantum Hall state in monolayer graphene. *Physical Review B* **2012**, *85*, 155439.
- (49) Checkelsky, J. G.; Li, L.; Ong, N. P. Zero-Energy State in Graphene in a High Magnetic Field. *Physical Review Letters* **2008**, *100*, 206801.

- (50) Nomura, K.; Ryu, S.; Lee, D.-H. Field-Induced Kosterlitz-Thouless Transition in the $N = 0$ Landau Level of Graphene. *Physical Review Letters* **2009**, *103*, 216801.
- (51) Kosterlitz, J. M. The critical properties of the two-dimensional xy model. *Journal of Physics C: Solid State Physics* **1974**, *7*, 1046–1060.
- (52) Liu, X.; Farahi, G.; Chiu, C.-L.; Papic, Z.; Watanabe, K.; Taniguchi, T.; Zaletel, M. P.; Yazdani, A. Visualizing broken symmetry and topological defects in a quantum Hall ferromagnet. *Science* **2022**, *375*, 321–326.
- (53) Coissard, A.; Wander, D.; Vignaud, H.; Grushin, A. G.; Repellin, C.; Watanabe, K.; Taniguchi, T.; Gay, F.; Winkelmann, C. B.; Courtois, H.; Sellier, H.; Sacépé, B. Imaging tunable quantum Hall broken-symmetry orders in graphene. *Nature* **2022**, *605*, 51–56.
- (54) Das, A.; Kaul, R. K.; Murthy, G. Coexistence of Canted Antiferromagnetism and Bond Order in $\nu = 0$ Graphene. *Physical Review Letters* **2022**, *128*, 106803.
- (55) Delagrangé, R.; Garg, M.; Breton, G. L.; Zhang, A.; Dong, Q.; Jin, Y.; Watanabe, K.; Taniguchi, T.; Roulleau, P.; Maillet, O.; Roche, P.; Parmentier, F. D. Vanishing bulk heat flow in the $\nu = 0$ quantum Hall ferromagnet in monolayer graphene. *Nature Physics* **2024**, *20*, 1927–1932.
- (56) Chiappini, F.; Wiedmann, S.; Novoselov, K.; Mishchenko, A.; Geim, A. K.; Maan, J. C.; Zeitler, U. Lifting of the Landau level degeneracy in graphene devices in a tilted magnetic field. *Physical Review B* **2015**, *92*, 201412.
- (57) Amet, F.; Bestwick, A. J.; Williams, J. R.; Balicas, L.; Watanabe, K.; Taniguchi, T.; Goldhaber-Gordon, D. Composite fermions and broken symmetries in graphene. *Nature Communications* **2015**, *6*, 5838.
- (58) Fertig, H. A.; Brey, L.; Côté, R.; MacDonald, A. H. Charged spin-texture excitations and

- the Hartree-Fock approximation in the quantum Hall effect. *Physical Review B* **1994**, *50*, 11018–11021.
- (59) Chatterjee, S.; Bultinck, N.; Zaletel, M. P. Symmetry breaking and skyrmionic transport in twisted bilayer graphene. *Physical Review B* **2020**, *101*, 165141.
- (60) Schmeller, A.; Eisenstein, J. P.; Pfeiffer, L. N.; West, K. W. Evidence for Skyrmions and Single Spin Flips in the Integer Quantized Hall Effect. *Physical Review Letters* **1995**, *75*, 4290–4293.
- (61) Pierce, A. T.; Xie, Y.; Lee, S. H.; Forrester, P. R.; Wei, D. S.; Watanabe, K.; Taniguchi, T.; Halperin, B. I.; Yacoby, A. Thermodynamics of free and bound magnons in graphene. *Nature Physics* **2022**, *18*, 37–41.
- (62) Atteia, J.; Lian, Y.; Goerbig, M. O. Skyrmion zoo in graphene at charge neutrality in a strong magnetic field. *Physical Review B* **2021**, *103*, 035403.
- (63) Piazza, V.; Pellegrini, V.; Beltram, F.; Wegscheider, W.; Jungwirth, T.; MacDonald, A. H. First-order phase transitions in a quantum Hall ferromagnet. *Nature* **1999**, *402*, 638–641.
- (64) Pan, C.; Wu, Y.; Cheng, B.; Che, S.; Taniguchi, T.; Watanabe, K.; Lau, C. N.; Bockrath, M. Layer Polarizability and Easy-Axis Quantum Hall Ferromagnetism in Bilayer Graphene. *Nano Letters* **2017**, *17*, 3416–3420.
- (65) Luo, W.; Côté, R. Transport gap and hysteretic behavior of the Ising quantum Hall ferromagnets in $|N| > 0$ Landau levels of bilayer graphene. *Physical Review B* **2014**, *90*, 245410.
- (66) Liu, L. et al. Observation of First-Order Quantum Phase Transitions and Ferromagnetism in Twisted Double Bilayer Graphene. *Physical Review X* **2023**, *13*, 031015.
- (67) Cho, H.; Young, J. B.; Kang, W.; Campman, K. L.; Gossard, A. C.; Bichler, M.; Wegscheider, W. Hysteresis and Spin Transitions in the Fractional Quantum Hall Effect. *Physical Review Letters* **1998**, *81*, 2522–2525.

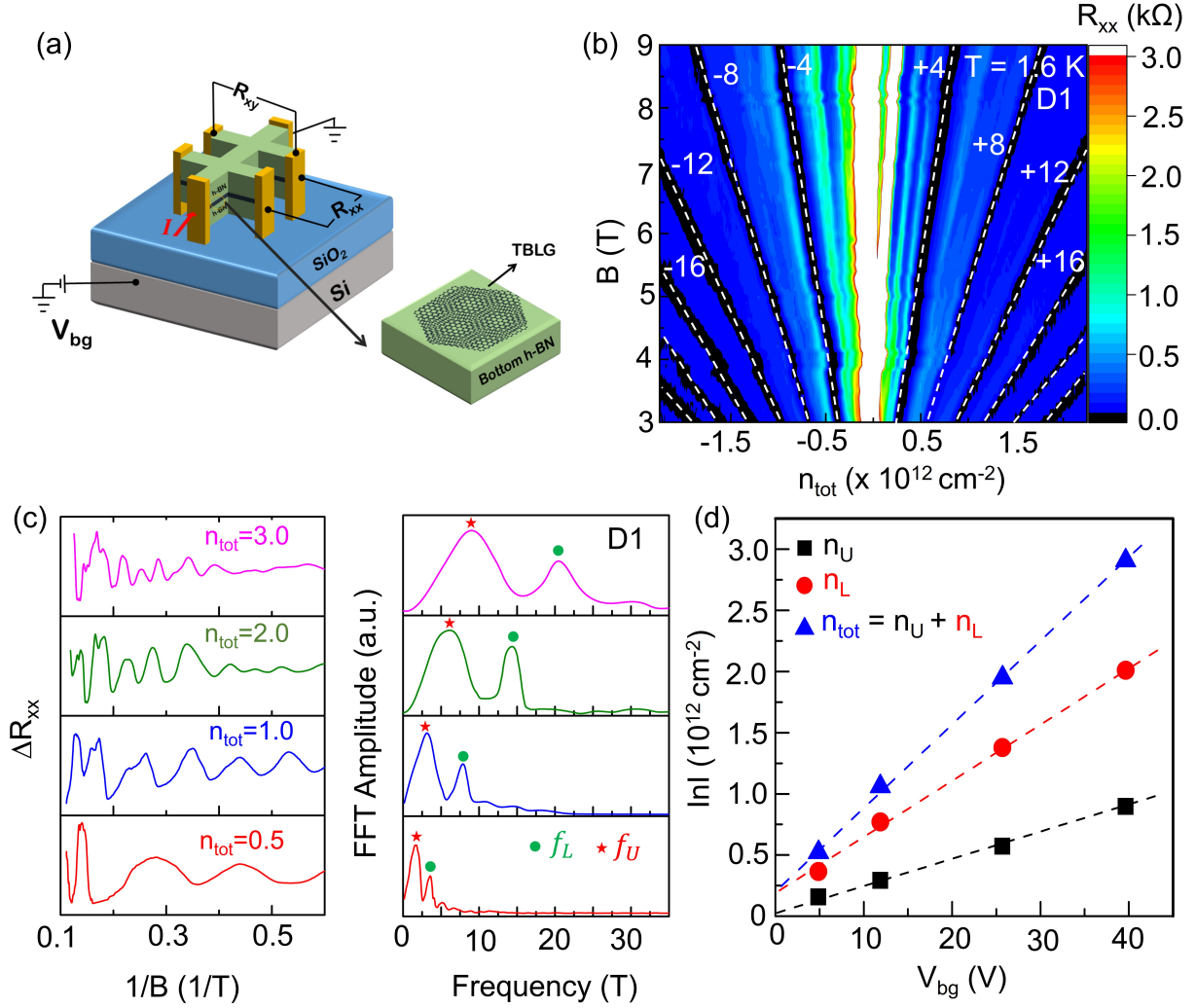


Figure 1: (a) Schematic illustration of the bottom-gated h-BN encapsulated TBLG in Hall bar geometry. (b) Landau fan diagram showing R_{xx} as a function of B and n_{tot} at 1.6 K. Different ν_{tot} values are shown in white dashed line. (c) ΔR_{xx} vs. $1/B$ for different n_{tot} ($\times 10^{12} \text{ cm}^{-2}$) values at 1.6 K (left) and corresponding FFT for each n_{tot} (right). (d) The upper layer (n_U), lower layer (n_L), and total (n_{tot}) carrier densities as function of gate voltage (V_{bg}). The dashed lines are the theoretical fits of graphene double layer model to experimental $|n|$ values estimated from FFT in (c).

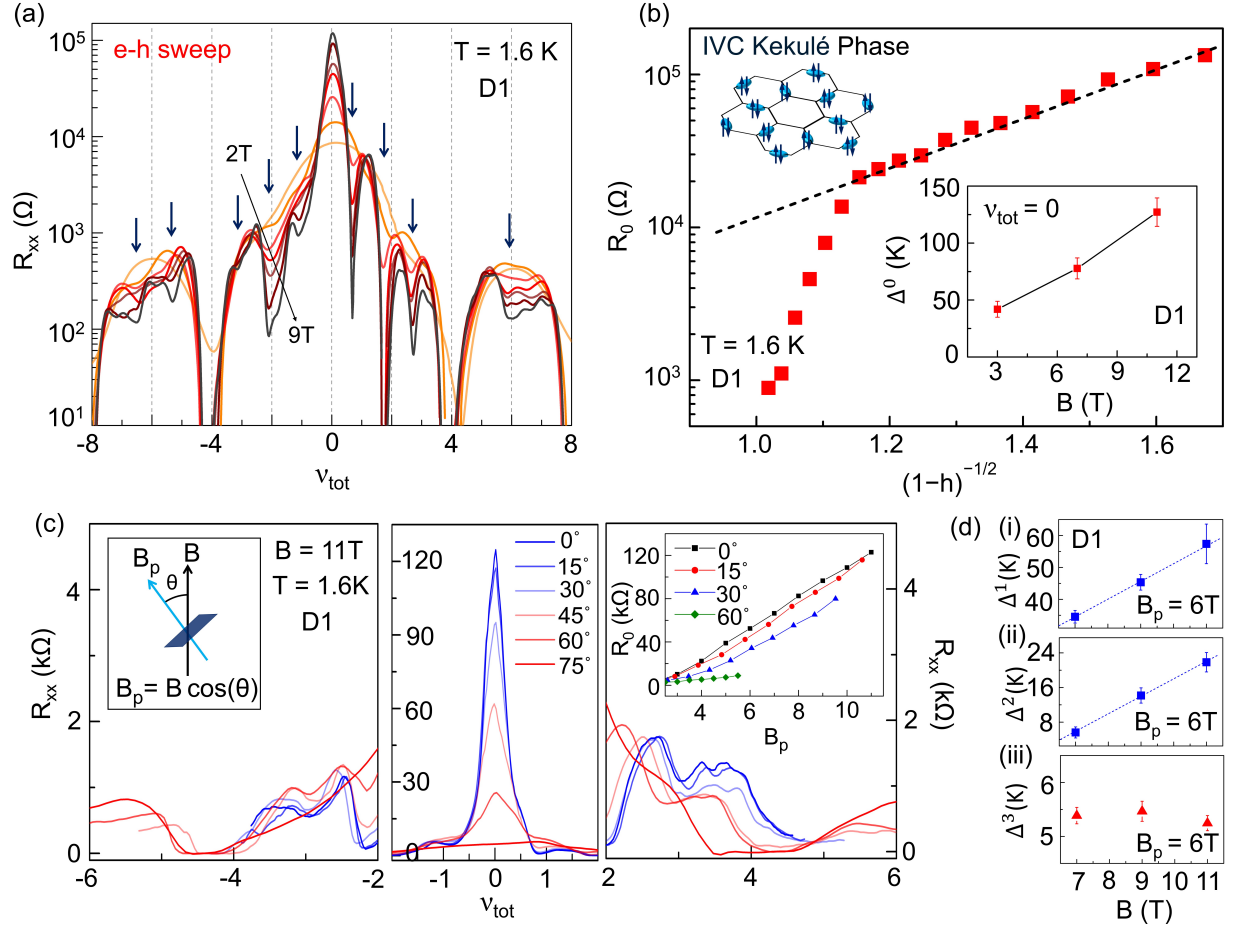


Figure 2: (a) Evolution of R_{xx} vs. ν_{tot} for e-h sweep at different B at 1.6 K with arrows indicating broken symmetry states. (b) R_0 (i.e., R_{xx} at $\nu_{\text{tot}} = 0$) vs. $(1-h)^{-1/2}$ fitted using the KT equation (dashed line). Insets: Activation gap at $\nu_{\text{tot}} = 0$, Δ^0 as a function of B and schematic of IVC Kekulé order phase. (c) R_{xx} vs. ν_{tot} for various tilt angles θ at $B = 11$ T as shown in left, center and right plots. Left inset: schematic of the tilted-field geometry. Right inset: R_0 vs. B_p at different θ . (d)(i)-(iii) Activation gaps Δ^{ν} vs. B for $\nu_{\text{tot}} = 1, 2, 3$, at fixed $B_p = 6$ T. The slope of the linear fit for each filling yields g_{\parallel} at the corresponding ν_{tot} .

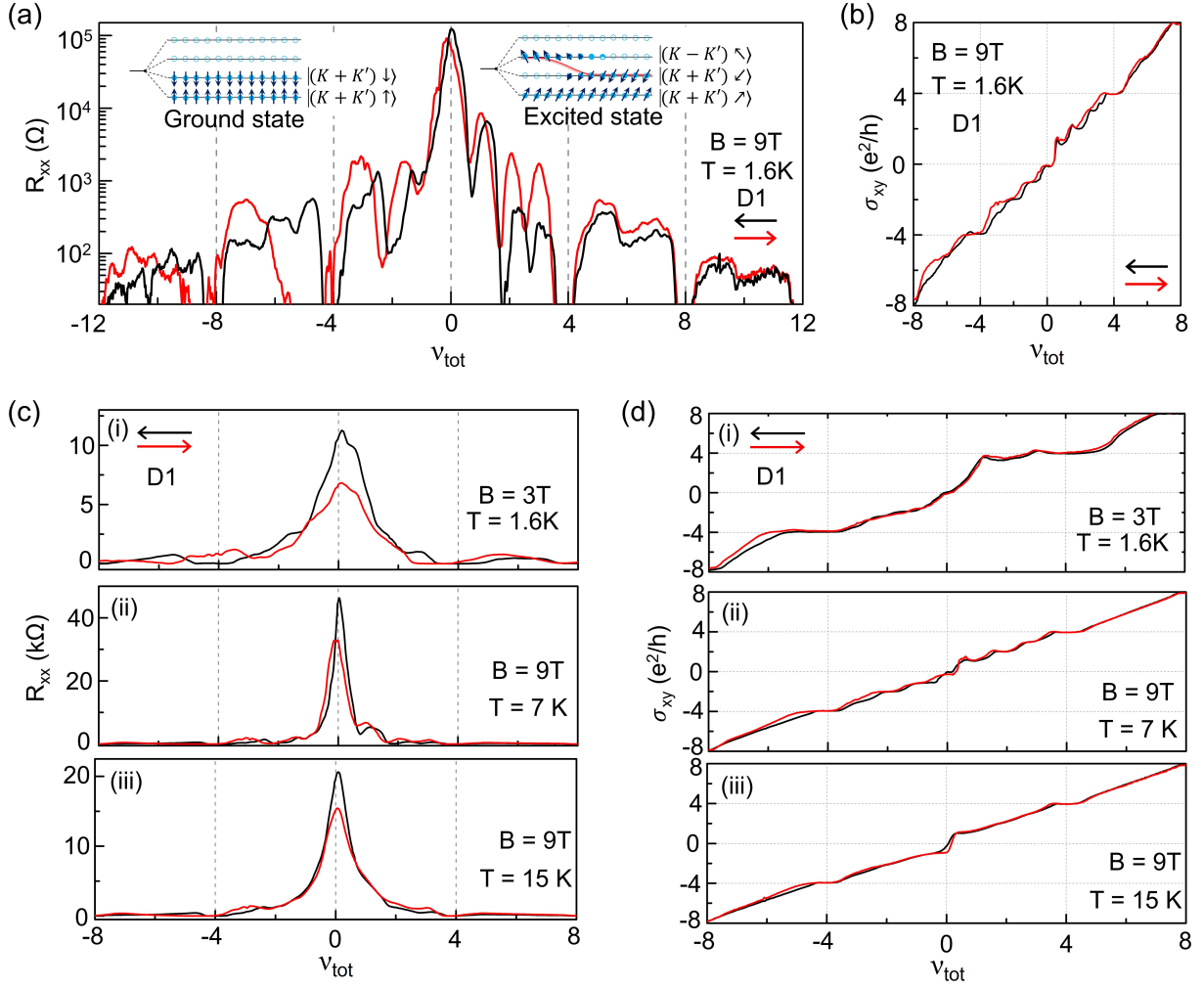


Figure 3: (a)-(b) Dual-sweep measurements of R_{xx} and σ_{xy} vs. v_{tot} at $B = 9T$ and $T = 1.6K$. Black and red arrows indicate the direction of the voltage sweep. The insets in (a) show ground and excited states of the $v_{tot} = 0$ IVC phase. (c) and (d) Dual-sweep measurements of R_{xx} and σ_{xy} as a function of total filling factor v_{tot} for D1 under three conditions: (i) $B = 3T$, $T = 1.6K$ (ii) $B = 9T$, $T = 7K$ and (iii) $B = 9T$, $T = 15K$.

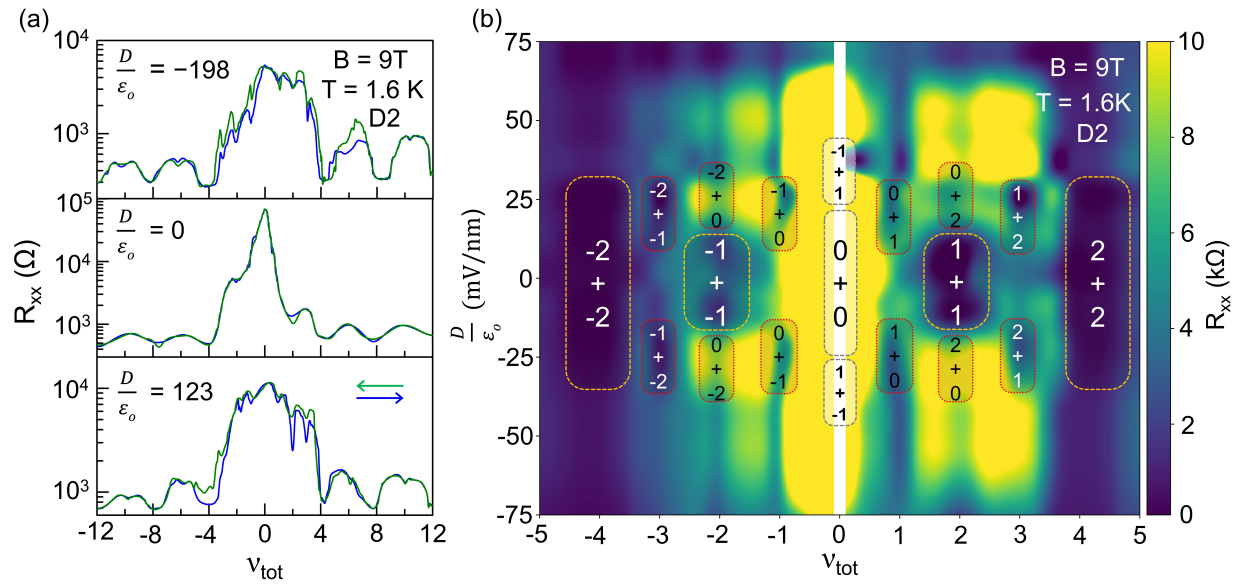


Figure 4: (a) Dual-sweep R_{xx} vs. v_{tot} at several D/ϵ_0 (in unit of mV/nm) for D2 at $B = 9$ T and $T = 1.6$ K indicating broken symmetry states and hysteresis. (b) Contour plot of R_{xx} vs. D/ϵ_0 and v_{tot} for D2 at $B = 9$ T and $T = 1.6$ K. The LL filling contributions from the upper and lower layers ($v_U + v_L$) are illustrated.

Supplemental Material

Skyrmionic Transport and First Order Phase Transitions in Twisted Bilayer Graphene Quantum Hall Ferromagnet

Vineet Pandey,[†] Prasenjit Ghosh,[†] Riju Pal,[‡] Sourav Paul,[†] Abhijith M B,[†] Kenji Watanabe,[§] Takashi Taniguchi,^{||} Atindra Nath Pal,[‡] and Vidya Kochat,^{*,†}

[†]*Materials Science Centre, Indian Institute of Technology, Kharagpur, West Bengal – 721302, India*

[‡]*S. N. Bose National Centre for Basic Sciences, Kolkata, West Bengal- 700106, India.*

[§]*Research Center for Electronic and Optical Materials, National Institute for Materials Science, 1-1 Namiki, Tsukuba 305-0044, Japan*

^{||}*Research Center for Materials Nanoarchitectonics, National Institute for Materials Science, 1-1 Namiki, Tsukuba 305-0044, Japan*

*E-mail: vidya@matsc.iitkgp.ac.in

S1. Experimental Methods

Raman Measurements: Raman scattering was performed using a WITec alpha300 system equipped with a 532 nm diode laser (~ 16.87 mW), (500 nm) spot size), 1800 lines/mm grating, and a 100X objective lens (NA = 0.95). Data analysis was carried out using WITec Project software and used to identify the twist angle of TBLG samples.

Device Fabrication: Single-layer graphene (SLG) and hexagonal boron nitride (h-BN) were obtained via mechanical exfoliation of bulk crystals. The h-BN layer was picked up using a PPC/PDMS stamp. TBLG samples were fabricated using the dry transfer method (Cryonano Labs) by sequentially picking up and transferring the top and bottom graphene layers onto pre-exfoliated h-BN on SiO₂/Si substrate. Devices with edge-contacted Hall bar geometry were patterned using e-beam lithography, followed by CF₄ and O₂ plasma etching of h-BN and graphene. Gold (Au) electrodes (70 nm) were deposited with a titanium (Ti) adhesion layer (10 nm) under a base pressure of 10^{-8} mbar in the thermal evaporation chamber.

Transport Measurements: Longitudinal (R_{xx}) and transverse (R_{xy}) resistance measurements were performed using a standard lock-in amplifier with an excitation frequency of $f = 17.77$ Hz and a current of $I = 10$ nA, and gate voltage was varied using Keithley 2450 SMU. These experiments were conducted in a Cryostat system (Cryogenics UK) equipped with a superconducting magnet capable of reaching fields up to 9 T.

S2. Raman Spectroscopy of twisted bilayer graphene

The twist angle (θ) of the twisted bilayer graphene (TBLG) devices were identified using Raman spectroscopy. Previous Raman studies have established that the R and R' modes, associated with LO phonons, exhibit a strong dependence on the twist angle [1,2]. Fig. S2(a) presents the optical images of devices D1, D2 and D3. The corresponding Raman maps focused on 2D-peak highlight the overlap regions (dashed outlines) where two monolayer graphene layers form the TBLG system, as shown in Fig. S2(b). The Raman spectra for devices D1, D2 and D3 are displayed in Fig. S2(c). For devices D1 and D2, we observed the R' mode around 1618 cm^{-1} and 1630 cm^{-1} , which corresponds to a twist angle of approximately 5° and 8° respectively.² Similarly, for device D3, the R mode was detected around 1426 cm^{-1} , indicating a twist angle of approximately 18° .

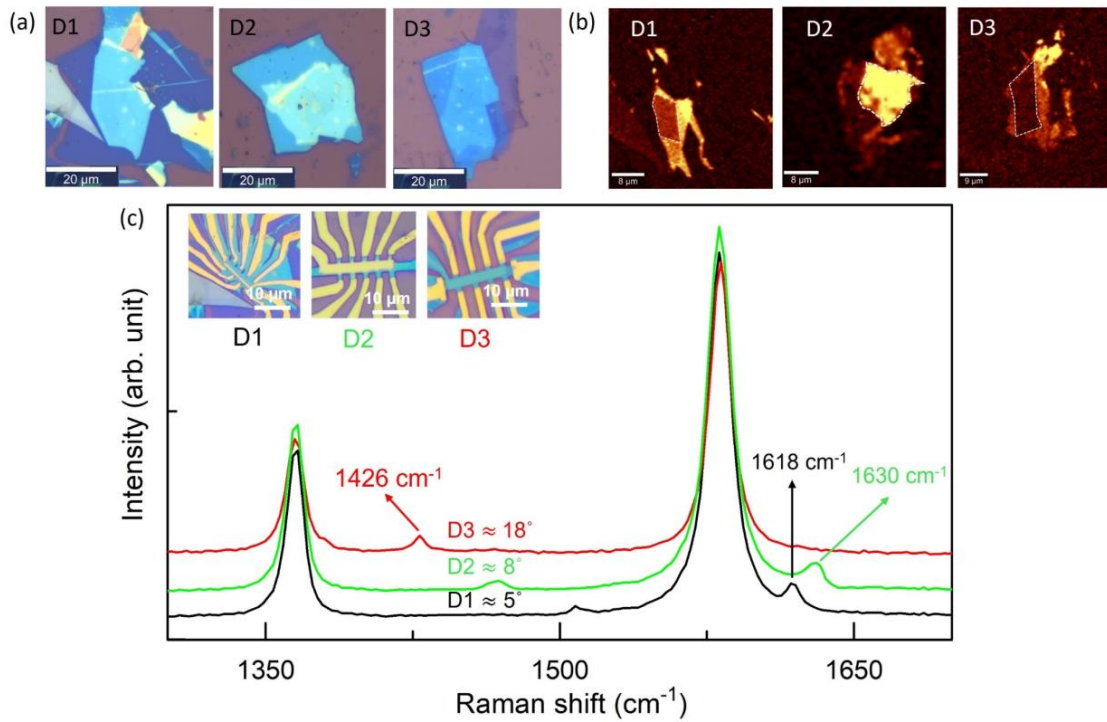


Figure S2: (a) Optical images of device D1, D2 and D3. (b) Raman map of TBLG device samples. (c) Raman spectra of devices D1, D2 and D3, and its optical images (Inset).

S3. Shubnikov-de Haas (SdH) measurements for D1

Fig. S3(a) shows the longitudinal (R_{xx}) and Hall (R_{xy}) resistances vs total filling factor (ν_{tot}) measured at $B = 9\text{ T}$ and $T = 1.6\text{ K}$ for device D1, illustrating the emergence of distinct quantum Hall (QH) states in the TBLG system. Fig. S3(b) to (e) present the SdH oscillations and corresponding QH plateaus observed at different total carrier densities (n_{tot}) for D1 at $T = 1.6\text{ K}$. The appearance of well-defined SdH oscillations and quantized Hall plateaus confirms the formation of Landau levels and the high quality of the TBLG device.

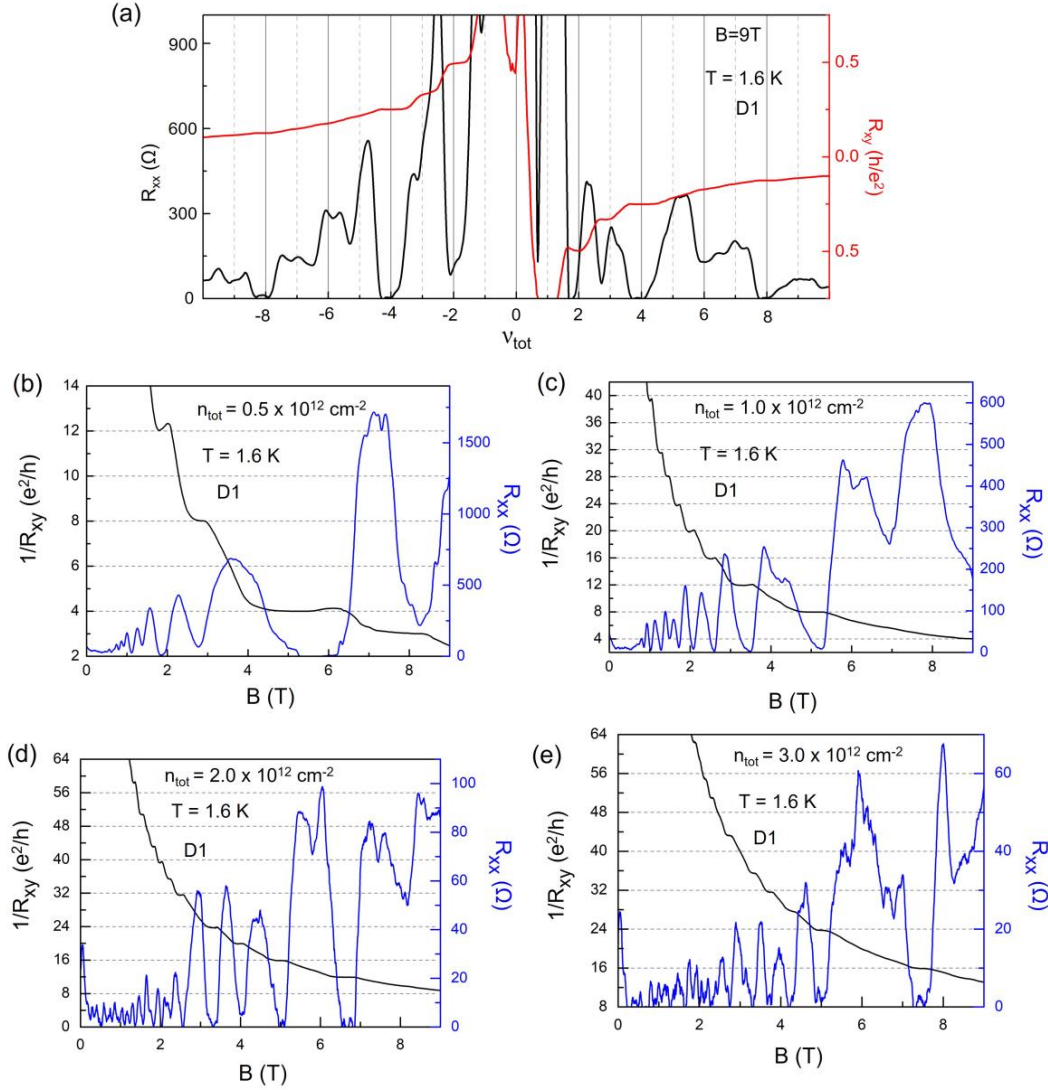


Figure S3: (a) Shows R_{xx} and R_{xy} vs. ν_{tot} for D1 at $B = 9T$ and $T = 1.6 K$. (b)-(e) shows plot of SdH oscillations for different n_{tot} values at $T = 1.6 K$ for D1.

S4. Calculation of filling factors of upper (ν_U) and lower (ν_L) layers

The schematic in Fig. S4(a) illustrates the LL filling in the lower and upper layers. Due to interlayer asymmetry, LLs in the upper layer are energetically less favourable in bottom gated TBLG devices, requiring additional charging energy for occupation. Once the first LL in the lower layer is filled, making it incompressible, subsequent carriers are forced to populate the LLs in the upper layer. Depending on the interplay between the charging energy of the upper layer and the LL gap in the lower layer, the next LL in the lower layer may become compressible before or after the upper layer LL is fully filled.

To investigate how the upper (n_U) and lower (n_L) layer densities vary with V_{bg} in TBLG samples, we employ a model designed to calculate the layer densities in graphene double layers that are independently contacted and separated by a dielectric medium [3]. The applied V_{bg} is

distributed between the SiO₂ dielectric and the Fermi energy of the lower graphene layer, described as:

$$e(V_{bg} - V_D) = \frac{e^2(n_U + n_L)}{C_{BG}} + E_F(n_L) \dots \dots \dots (1)$$

where, V_D is the Dirac point offset and C_{BG} is the back-gate capacitance of SiO₂ and h-BN. The Fermi energy relative to the charge neutrality point in monolayer graphene at a carrier density n is given by $E_F(n) = \text{sgn}(n) \hbar v_f \sqrt{\pi |n|}$, where $\text{sgn}(n)$ is signum function and determines the sign of n , and the Fermi velocity is given as $v_f \approx 10^8$ cm/s. The E_F of the lower layer can be expressed as the sum of the electrostatic potential difference between the layers and the Fermi energy of the upper layer:

$$E_F(n_L) = \frac{e^2 n_U}{C_{int}} + E_F(n_U) \dots \dots \dots (2)$$

where C_{int} is the interlayer capacitance between two layers of TBLG. For device D1, experimental $n_{U,L}$ vs. V_{bg} calculated using FFT analysis of SdH data (Fig. 1(e)) in main text is linearly fitted with the equation (2), gives interlayer capacitance of $C_{int} = (5.7 \pm 1)$ $\mu\text{F}/\text{cm}$ as a fitting parameter, which agrees with the theoretically expected interlayer capacitance of Bernal-stacked bilayer graphene [3,4]. By using Eqs. (1) and (2) and using $C_{int} = 5.7$ $\mu\text{F}/\text{cm}$, we calculated n_U and n_L and the corresponding $n_{tot} (= n_U + n_L)$. The plot for $n_{U,L}$ vs n_{tot} shown in Fig. S4(b). The Fermi energy depends on both carrier density and magnetic field and is given by $E_F = E_N$, where $E_N = \text{sgn}(N) v_f \sqrt{2e\hbar B |N|}$ is the energy of the N^{th} Landau level (LL) in TBLG. Here, $N = \text{Int} \left[\frac{nh}{4eB} \right]$ represents the LL index, with Int denoting the nearest integer function. Using n_U and n_L densities we calculated layer filling factors $\nu_{U,L} = \frac{n_{U,L} \hbar}{eB}$. The plot $\nu_{U,L}$ vs n_{tot} for 3T, 6T and 9T is shown in Fig. S4(c).

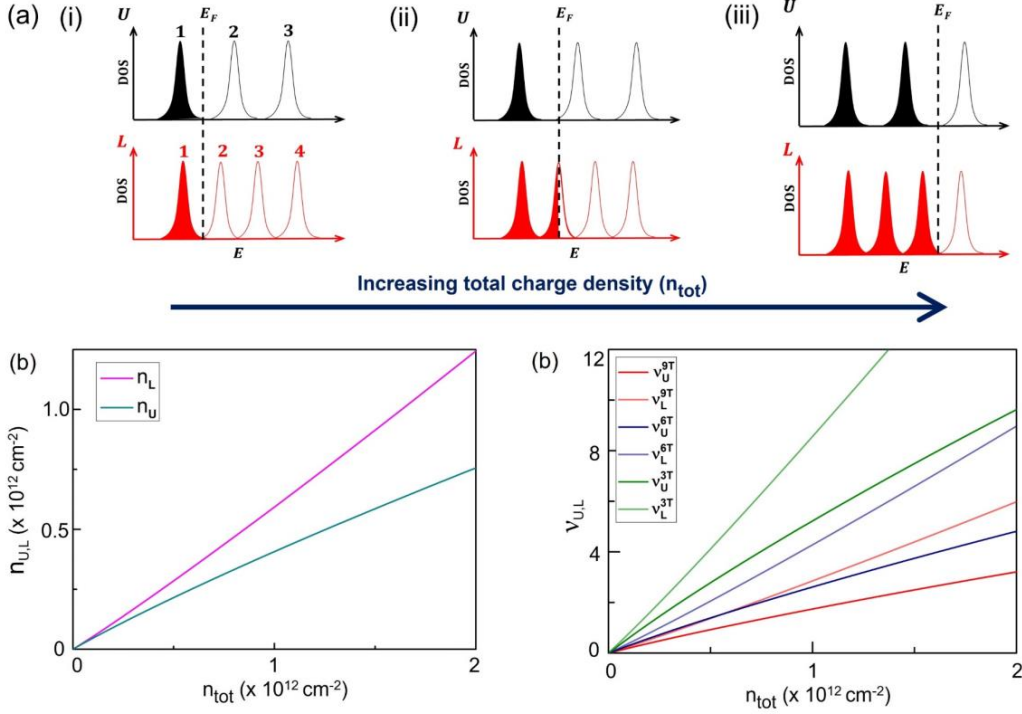


Figure S4: (a) Schematic illustrates the partial LL filling in the lower and upper layers due to charge screening effects. (b) Plot for calculated $n_{U,L}$ vs n_{tot} for D1. (c) Plot calculated $v_{U,L}$ vs n_{tot} at 3T, 6T and 9T for device D1.

S5: Arrhenius plots for different integer filling factors for device D1

Fig. S5(a) presents the Arrhenius plot of $\ln \rho_{xx}$ versus $1/T$ for $v_{tot} = 0$. Fig. S5(b), (c) and (d) show similar Arrhenius plots for $v_{tot} = 1, 2$, and 3 respectively for tilted field measurement done at fixed perpendicular magnetic field, $B_p = 6T$ for different total applied magnetic field (B). The data were analyzed using the Arrhenius relation,

$$\rho_{xx}(T) = \rho_0 \exp\left(\frac{\Delta^v}{2k_B T}\right),$$

where Δ^v represents the activation gap and k_B is the Boltzmann constant.

The slopes obtained from the linear fits in these plots were used to extract the values of Δ^v corresponding to different v_{tot} , as presented in the main manuscript.

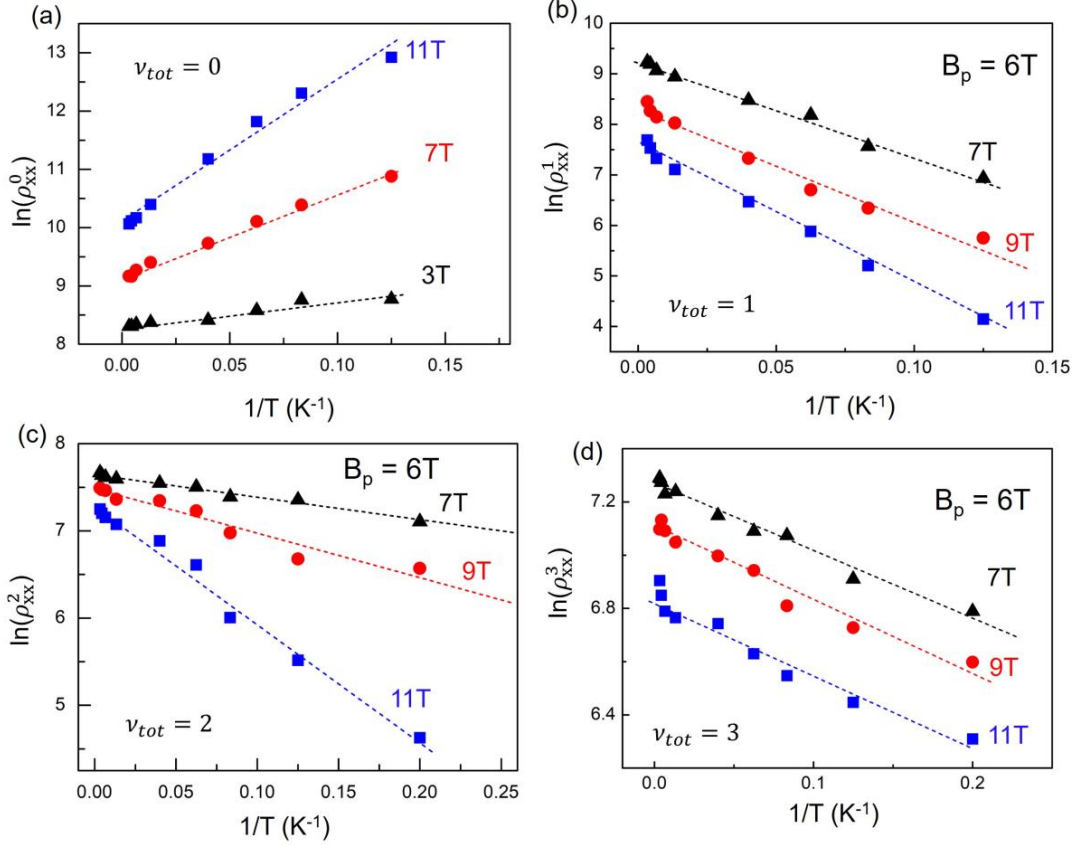


Figure S5: (a) Plot of $\ln \rho_{xx}$ versus $1/T$ for $\nu_{tot} = 0$ for D1. (b)-(d) Plot of $\ln \rho_{xx}$ versus $1/T$ for $\nu_{tot} = 1, 2$ and 3 for fixed $B_p = 6T$ for D1.

S6: Effect of zero and finite displacement field in device D2

To investigate the origin of hysteretic behaviour in TBLG, we fabricated a dual-gated device (D2) with an estimated twist angle of approximately 8° . This configuration allows independent control over the total carrier density (n_{tot}) and the interlayer displacement field (D). The n_{tot} for dual gated TBLG system is given by:

$$e \cdot n_{tot} = C_T V_{tg} + C_B V_{bg},$$

where C_T and C_B are the capacitance per unit area of the top and bottom gates, respectively, V_{tg} and V_{bg} , are the respective gate voltages, and e is the elementary charge. The displacement field (D) between the two graphene layers, is defined as:

$$D = \frac{C_T V_{tg} - C_B V_{bg}}{2}$$

In our twisted bilayer graphene sample, the resistance at the charge neutrality points (CNP) decreases almost linearly with increasing displacement field D , in contrast to AB-stacked bilayer graphene where D breaks inversion symmetry and opens a band gap. This behavior

rules out AB stacking and is instead consistent with D inducing equal and opposite charge doping in the two layers, thereby lowering the resistance of each layer as shown in Fig. S6(a). Because of the finite interlayer gap, the bottom layer partially screens the gate field, reducing the charge that reaches the top layer, which in turn modifies how Landau levels are filled in both layers.

Fig. S6(a) shows R_{xx} vs n_{tot} measured at $B = 0$ T for different displacement field ($\frac{D}{\epsilon_0}$, in units of mV/nm) values (the curves have been offset along the density axis for better clarity). At the CNP, where $n_{tot} (= n_U + n_L) = 0$, the two graphene layers contribute in parallel to the total resistance. Because the layers conduct in parallel, $R_{xx}^{-1} \approx R_U^{-1} + R_L^{-1}$, the total resistance at CNP decreases systematically as $|\frac{D}{\epsilon_0}|$ increases, as n_U and n_L changes in individual layers. At sufficiently large displacement fields, the density difference between the layers becomes large enough that sweeping n_{tot} separately crosses the CNPs of the top and bottom layers. As a result, the single resistance peak at the CNP begins to split into two distinct peaks, each associated with one layer's neutrality point as shown in Fig. S6(a). Fig. S6(b) shows the contour plot of $\frac{D}{\epsilon_0}$ versus n_{tot} at $B=0$ T. At $\frac{D}{\epsilon_0} = 0$, only a single resistance peak is visible, reflecting the degenerate CNP of the two layers. With increasing $|\frac{D}{\epsilon_0}|$, this peak splits into two as shown in white dashed lines, directly revealing the separation of the individual layer neutrality points as the layers become energetically resolved. Furthermore, opposite gate-sweep directions at $B = 0$ T exhibit no noticeable hysteresis at any D (see Fig. S6(c)). The absence of hysteresis signifies that sweeping the gates doesn't put the device in any metastable charge state, i.e., there is negligible charge trapping or ferroelectric-like switching at zero field condition.

At $D/\epsilon_0 = 0$, single-sweep measurements of the R_{xx} as a function of v_{tot} , depicted in Fig. S6(d), reveal a distinct evolution with magnetic field. At low magnetic fields the spectrum displays an effective eight-fold Landau level degeneracy such that resistance minima appear at $|v_{tot}| = 4, 12, 20, \dots$, consistent with two nearly decoupled graphene monolayers where it shows 2 times of $|v_{tot}| = 2, 6, 10, \dots$. But when B is increased, the sequence reorganizes into a four-fold pattern with minima at $|v_{tot}| = 4, 8, 12, 16, \dots$ and so on. This evolution reflects broken symmetry QH states appear in each layer like $|v_{tot}| = 1, 2, 3, 4, \dots$, so that 2 times should give 4-fold degeneracy like $|v_{tot}| = 4, 8, 12, 16, \dots$. This behaviour aligns with previous studies indicating that stronger magnetic fields facilitate the emergence of four-fold quantum Hall ferromagnetic states at zero displacement field [5].

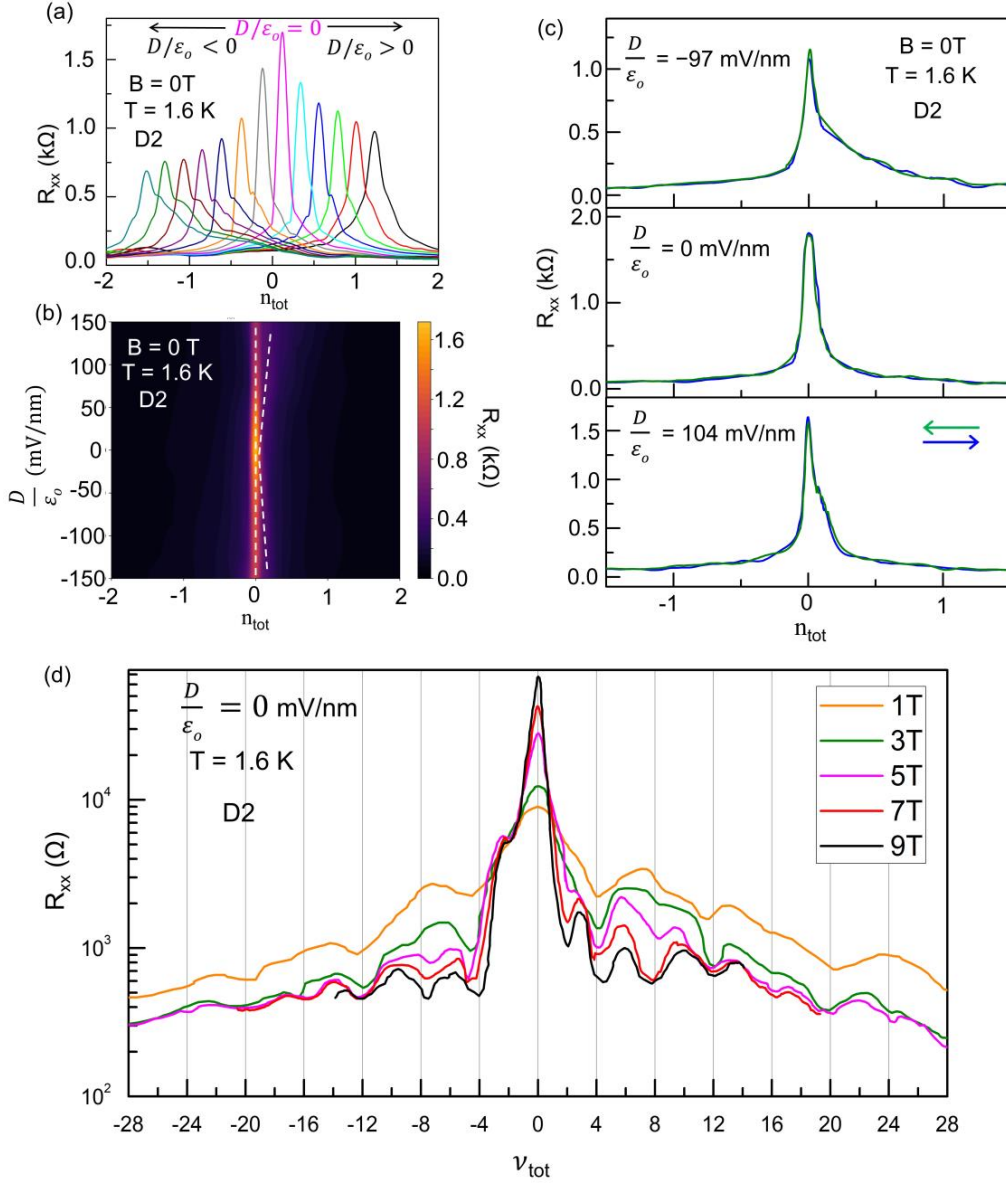


Figure S6: (a) R_{xx} vs n_{tot} at the CNP measured at $B=0$ T for different displacement field ($\frac{D}{\epsilon_0}$) values. The peak resistance at CNP decreases as $|\frac{D}{\epsilon_0}|$ increases. Curves are offset along the n_{tot} axis for peak split clarity. (b) $\frac{D}{\epsilon_0}$ vs v_{tot} contour plot for $B = 0$ T. Two splitting white dashed line shows the appearance of 2nd peak with increasing displacement field. (c) Dual-sweep R_{xx} vs. n_{tot} at several $\frac{D}{\epsilon_0}$ values for D2 at $B = 0$ T and $T = 1.6$ K. (d) R_{xx} vs v_{tot} at $\frac{D}{\epsilon_0} = 0$ at 1.6 K.

S7: QH states and hysteresis behaviour of device D3

Device D3 (i.e., $\theta \approx 18^\circ$) was characterized to explore the emergence of QH states and its magnetoresistance. Fig. S7(a) illustrates the longitudinal resistance (R_{xx}) as a function of total carrier density (n_{tot}) at 300 K and 1.6 K in the absence of a magnetic field (B). The device

exhibited low mobility ($\approx 18,000 \text{ cm}^2 \text{ V}^{-1} \text{ s}^{-1}$). Fig. S7(b) presents R_{xx} versus the total filling factor (ν_{tot}) at 1.6 K under varying B. Similar to Device D1, R_{xx} increases at $\nu_{tot} = 0$ as B increases, but we do not observe a divergent behaviour till 9T. In device D3, broken-symmetry QH states were also not observed up to 9 T, likely due to the high disorder in the sample. Despite this low mobility and high disorder, QH states were observed at filling factors $\nu_{tot} = \pm 4, \pm 8, \pm 12, \pm 16 \dots$ similar to D1 and D2 (see main text).

Fig. S7(c) and S7(d) present the magnetic field (B) and temperature (T) dependence, respectively, of dual sweeps of R_{xx} as a function of ν_{tot} for Device D3. In the B-dependence data shown in Fig. S7(c), the emergence of QH states is observed with increasing magnetic field, consistent with the formation of Landau levels. However, the absence of notable hysteresis, in contrast to Device D1 and D2, suggests that hysteresis observed in D1 and D2 is most certainly due to the QH ferromagnetism arising from the broken symmetry states and its skyrmionics behaviours.

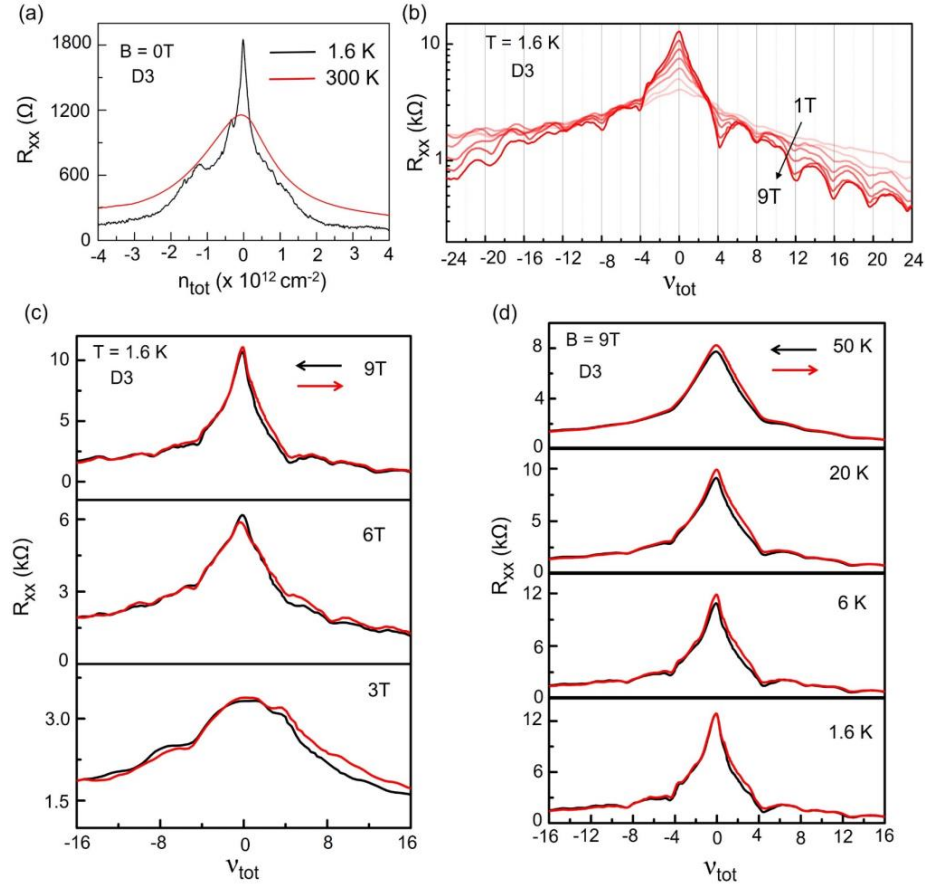


Figure S7: Transport characterization of Device D3 ($\theta \approx 18^\circ$). (a) R_{xx} as a function of n_{tot} at 300 K and 1.6 K in zero magnetic field. (b) R_{xx} versus ν_{tot} at 1.6 K under varying magnetic field strengths. (c) Magnetic field dependence of dual sweeps showing R_{xx} as a function of ν_{tot} for D3. (d) Temperature dependence of dual sweeps showing R_{xx} as a function of ν_{tot} for D3.

S8: K-T transition analysis in device D2

We applied the Kosterlitz–Thouless (K–T) fitting procedure to device D2. The plot of $\log R_0$ vs. $\sqrt{1-h}$ shows that D2 exhibits a sharper and rapid resistivity increase associated with the K–T transition as shown in Fig. S8(a). From the fits we obtain critical field for ordered state, $B_C = 16T$. This value is derived from the plot of $\left(\frac{d \ln R_0}{dH}\right)^{-2/3}$ versus B , as shown in Fig. S8(b). The slope, $b \sim 0.72$, aligns closely with established KT theory. The derived $B_C = 12T$ for device D1 also shown in Fig. S8(c).

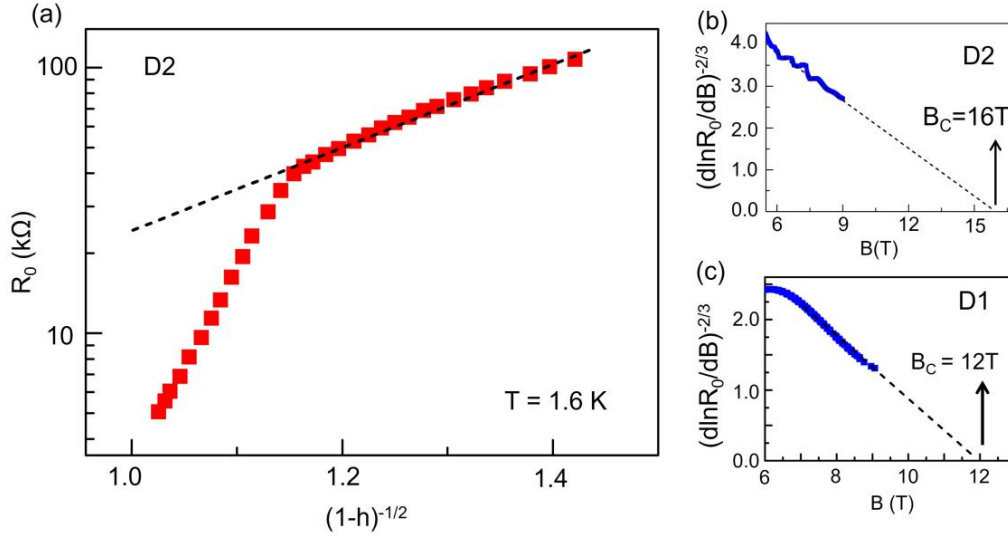


Figure S8: (a) K-T analysis for device D2. Plot shows $\log R_0$ vs. $\sqrt{1-h}$. Slope calculated $b \sim 0.72$ for $B_C = 16T$, derived from the plot of $\left(\frac{d \ln R_0}{dH}\right)^{-2/3}$ vs. B as shown in (b). (c) Plot of $\left(\frac{d \ln R_0}{dH}\right)^{-2/3}$ vs. B for device D1 shows the $B_C = 12T$.

References

1. V. Carozo, C. M. Almeida, E. H. M. Ferreira, L. G. Cançado, C. A. Achete, and A. Jorio, *Nano Letters* **11**, 4527 (2011).
2. V. Pandey, S. Mishra, N. Maity, S. Paul, A. M. B, A. K. Roy, N. R. Glavin, K. Watanabe, T. Taniguchi, A. K. Singh, and V. Kochat, *ACS Nano* **18**, 4756 (2024).
3. B. Fallahazad, Y. Hao, K. Lee, S. Kim, R. S. Ruoff, and E. Tutuc, *Physical Review B* **85**, 201408 (2012).
4. H. Schmidt, T. Lüdtkke, P. Barthold, E. McCann, V. I. Fal'ko, and R. J. Haug, *Applied Physics Letters* **93** (2008), 10.1063/1.3012369.
5. J. D. Sanchez-Yamagishi, T. Taychatanapat, K. Watanabe, T. Taniguchi, A. Yacoby, and P. Jarillo-Herrero, *Physical Review Letters* **108**, 076601 (2012).